JOURNAL OF APPLIED ELECTROCHEMISTRY 20 (1990) 996–999

AC-Impedance measurements on aluminium in chloride containing solutions and below the pitting potential

S. E. FRERS, M. M. STEFENEL, C. MAYER, T. CHIERCHIE

Laboratorio de Ingenreria Electroquímica, Dpto. de Quimica e Ingenreria Química, Universidad Nacional del Sur, Aven Alem 1253, (8000) Bahia Blanca, Argentina

Received 21 February 1990

Impedance measurements were performed on aluminium in 0.5 M NaCl in the frequency range 5×10^{-4}–10^4 Hz and before the onset of pitting corrosion. The behaviour of the system was characterized by a high frequency capacitive loop related to the thickness of the oxide film, an inductive loop at medium frequency, which was interpreted on the basis of the dielectric relaxation model proposed by Dignam, and a second capacitive loop obtained at low frequencies which was ascribed to the film dissolution through the formation of a soluble chloride containing aluminium salt.

1. Introduction

The passivity of metals is a well-known phenomenon which has been extensively studied because of its theoretical and practical importance [1–7]. Passive metals corrode through consecutive processes occurring at the metal/oxide interface, in the oxide film and at the oxide film/solution interface. Much effort has been devoted to determine the mechanism of passive film growth [8–11].

The passive behaviour of aluminium in aqueous solution is strongly affected by the nature of the electrolyte. Depending on the electrode potential, in solutions containing aggressive anions such as Cl^-, a localized metal dissolution is initiated at those sites where the film breaks down. However, the behaviour of the passive film below the pitting potential has not been studied in detail.

The aim of the present work is to shed some light on the fundamental processes occurring on the aluminium passive layer in Cl^- containing neutral solutions. Electrochemical studies were performed using the a.c. impedance technique with measurements taken over a wide frequency range in order to obtain sufficient meaningful faradaic information.

2. Experimental details

Measurements were carried out in a three-compartment cell. The working electrode was a 4N purity aluminium rod sealed into a Teflon holder with epoxy resin in order to expose only the top surface of the metal to the solution. A platinum sheet and a saturated calomel electrode (SCE) connected to the cell by a Luggin capillary served as counter and reference electrodes respectively. Both were separated from the main compartment of the cell by fine-pored glass diaphragms.

All measurements were performed in 0.5 M NaCl solutions prepared from analytical grade chemicals and triply distilled water.

The electronic circuitry consisted of a Solartron Electrochemical Interface 1286 and a Solartron Frequency Response Analyzer 1250 coupled to a Hewlett Packard computer 9216. Over the frequency range studied, 5×10^{-4}–10^4 Hz, the amplitude of the a.c. signal was kept constant, $\Delta E = 14$ mV.

In order to obtain reproducible and comparable results, special attention was paid to the surface pretreatment. After trying different methods, the most accurate results were achieved by mechanical polishing of the electrode surface up to a mirror finish, followed by immersion in a NaOH solution.

3. Results and discussion

Figure 1 shows a current–potential curve for aluminium in 0.5 M NaCl, obtained by applying a linear potential perturbation at a sweep rate, $v = 10^{-4}\,V\,s^{-1}$. Within the potential range of passivity a small anodic dissolution current, which is slightly potential-dependent is observed. Beyond this region a strong potential-dependent dissolution current, various orders of magnitude larger than the passive current, indicates the onset of pitting corrosion. In order to avoid complication due to the superposition of either hydrogen evolution or pitting corrosion, a.c. measurements were restricted to the potential range $-1.05\,V \leqslant E \leqslant -0.80\,V$. Before each measurement, the electrode was kept at a constant potential until reaching a steady-state current value. Figure 1 (inserted subdiagram) shows a steady-state polarization curve within the passive region.

The reliability of experimental data when applying a.c. impedance measurements in electrochemical systems, depends mainly on the fulfilment of two conditions: the linearity and the stability of the system.

0021-891X/90 $03.00 + .12

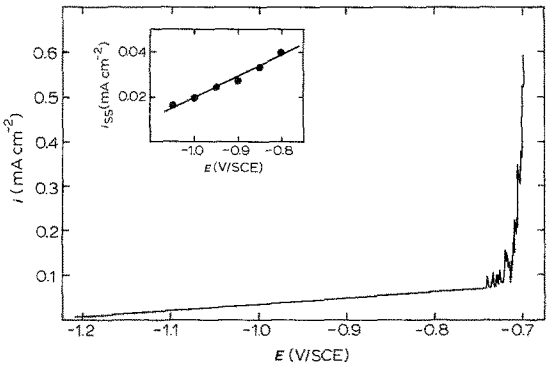

Fig. 1. Current-potential curve for aluminium in 0.5 M NaCl at $v = 10^{-4}\,V\,s^{-1}$. Insert: steady-state polarization curve within the passive region.

Measurements carried out up to $\Delta E = 20\,mV$ were independent of the magnitude of the perturbating signal. This ensured a linear behaviour of the system at $\Delta E = 14\,mV$, the value used herein. The second condition implies that the system returns to its initial state after removing the perturbation. This requirement is especially important when working at very low frequencies. For the frequency range employed in this work each measurement required about 24 h, however, after removing the a.c. signal the steady-state current differed from the initial current by less than $\pm 5\%$. This enabled both reproducible as well as comparable results to be obtained over the whole frequency range.

A set of Nyquist plots obtained at different potentials are given in Fig. 2. In order to show the main features of the complex diagram, the experimental points are restricted to $f \geqslant 5 \times 10^{-3}$ Hz. In all cases three loops were obtained: (a) a capacitive loop at high frequencies, (b) an inductive loop at medium frequencies and (c) a second capacitive loop at low frequencies.

The experimental results were interpreted in terms of the electric equivalent circuit in Fig. 3a which describes the impedance diagrams over the whole potential range studied. R_1, R_2, R_3, C and L are related to the faradaic impedance, while C^* represents the capacity of the metal/film/electrolyte interface. The electrolyte resistance was omitted since it was found to

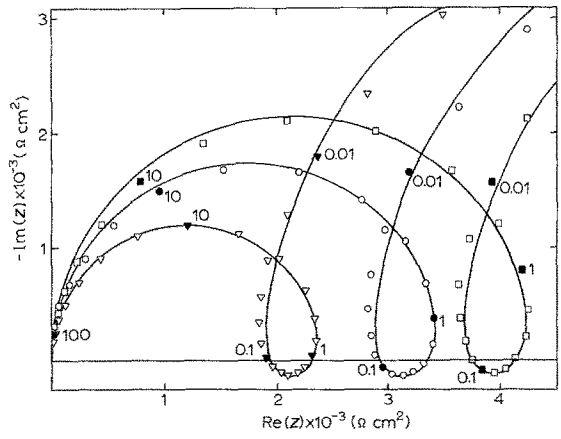

Fig. 2. Simulated (——) and experimental impedance diagrams for aluminium in 0.5 M NaCl obtained at different potentials: (▽) −0.8 V, (○) −0.9 V and (□) −1.0 V. Frequencies in Hz.

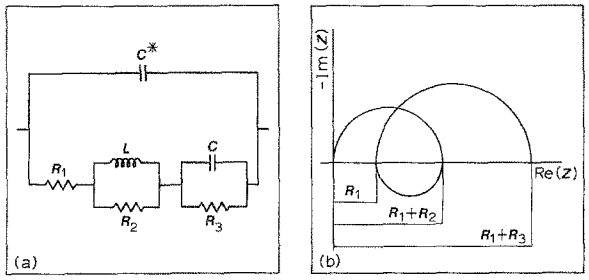

Fig. 3. (a) Equivalent circuit for the total electrode impedance. (b) Complex impedance diagram for the circuit in (a) when $1/CR_3 < R_2/L$.

be in the order of $3\,\Omega cm^2$, which is negligible in comparison with the impedance values shown in Fig. 2.

According to the circuit in Fig. 3a, the faradic (Z_F) and the total (Z) impedance are related by

$$1/Z = sC^* + (1/Z_F) \quad (s = j\omega) \tag{1}$$

with

$$Z_F = Z_1 + Z_2 \tag{2}$$

$$Z_1 = R_1 + R_2 + \frac{(-R_2^2/L)}{s + (R_2/L)} \tag{3}$$

$$Z_2 = \frac{1/C}{s + 1/CR_3} \tag{4}$$

A schematic representation for Z in the complex plane is given in Fig. 3b.

For each experimental curve, values of R_1, R_2, R_3, C^*, C and L (Table 1) were obtained by a computer fitting procedure carried out on a VAX-11/780 computer using the FORTRAN IV program BMDPAR. Figure 2 shows a good agreement between experimental and simulated data.

As a first approximation, the capacitance C^* may be related to a series connection between the double layer capacity (C_{dl}) and the oxide layer capacity (C_{ox}) according to the usual expression

$$1/C^* = 1/C_{dl} + 1/C_{ox} \tag{5}$$

where $C_{ox} = \varepsilon\varepsilon_0/\delta_{ox}$, with ε_0 the permittivity of the free space, ε the dielectric constant of the oxide and δ_{ox} its thickness. Since C_{ox} diminishes with increasing oxide film thickness, the total capacity C^* should decrease with increasing electrode potential in agreement with the results given in Table 1. Taking $C_{dl} = 50\,\mu F\,cm^{-2}$ and $\varepsilon = 9$ [12] the linear potential dependence of δ_{ox} on E was obtained. The values for this, given in Fig. 4, indicate the presence of a thin barrier oxide film.

The inductive loop observed at medium frequencies has already been reported on thin [13] and thick [10] aluminium oxide layers grown in non-aggressive electrolytes, as well as on passive iron in acid medium [14]. This inductive behaviour has been observed during galvanostatic and potentiostatic transient measurements on aluminium and other valve metals (see [7] and references therein) and it may be related to relaxation processes within the oxide film. In the following description Dignam's dielectric relaxation model [3, 7, 8] was adopted to explain the results presented in

Table 1. Potential dependence of the fitted parameters

E (V)	R_1 (Ωcm^2)	R_2 (Ωcm^2)	R_3(Ωcm^2)	$C \times 10^3$ ($F cm^2$)	$C^* \times 10^6$ ($F cm^{-2}$)	L ($H cm^{-2}$)
−0.800	1900	508	7923	9.60	6.58	687
−0.850	2283	560	8413	10.16	7.21	994
−0.900	2863	634	7931	10.21	7.31	1519
−0.950	3108	632	7582	11.09	7.81	1681
−1.000	3654	668	7795	11.57	8.18	2110
−1.050	4246	699	7193	12.16	8.62	3129

this paper. This model has satisfactorily accounted for experimental results obtained on different valve metals.

According to this model the polarization, P, of the oxide film may be split into a fast component, $P_1 = \varepsilon_0 \chi_1 F$, which responds instantaneously to the field, F, and one or more slow components, P_k ($k = 2, 3, \ldots$) whose response occurs over a finite time. In the following account only P_2 will be considered. On the other hand if the rate of change of the slow polarization component is mainly controlled by the passage of ionic current, i.e. thermal activation is negligible, Dignam's model leads to the following equations:

$$i = A \exp \{\beta [(1 + \chi_1) F + P_2/\varepsilon_0]\} \quad (5)$$

$$\frac{dP_2}{dt} = B_2 i (\varepsilon_0 \chi_2 F - P_2) \quad (6)$$

where A and β are constants, B_2 is a measure of the interaction cross-sectional area for a moving defect, and $(1 + \chi_1)$ and $(1 + \chi_1 + \chi_2)$ are the dynamic and static dielectric constants of the film, respectively.

Under steady state conditions ($i = i_{ss}$ and $F = F_{ss}$) $dP_2/dt = 0$. That is,

$$\varepsilon_0 \chi_2 F_{ss} = P_{2ss} \quad (7)$$

According to Equation 5, the current is a function of F and P_2. Therefore, the current response δi to a perturbation $\delta F = F - F_{ss} = \Delta F \exp(st)$, with ΔF small enough for the system to fulfil the condition of linearity, is given by

$$i = \left(\frac{\partial i}{\partial F}\right)_{ss} \delta F + \left(\frac{\partial i}{\partial P_2}\right)_{ss} \delta P_2 \quad (8)$$

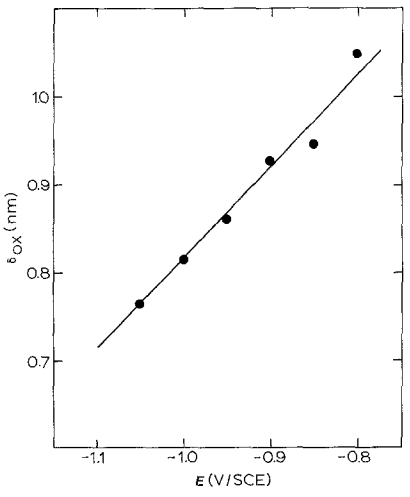

Fig. 4. Potential dependence of the oxide film thickness.

with

$$\delta i = i - i_{ss} = \Delta i \exp(st) \quad (9)$$

$$\delta P_2 = P_2 - P_{2ss} = \Delta P_2 \exp(st) \quad (10)$$

since $dP_2/dt = s\delta P_2$, substitution of Equations 7, 9 and 10 into Equation 6, and neglecting second order terms, yields:

$$\delta P_2 = B_2 i_{ss} \varepsilon_0 \chi_2 \frac{\delta F}{s + B_2 i_{ss}} \quad (11)$$

Substituting Equation 11 into Equation 8, and subsequent rearrangement, gives the following expression for the impedance

$$\frac{1}{Z_1} = \left(\frac{\partial i}{\partial F}\right)_{ss} + \frac{i_{ss} \varepsilon_0 \chi_2 B_2}{s + B_2 i_{ss}} \left(\frac{\partial i}{\partial P_2}\right)_{ss} \quad (12)$$

with $(\partial i/\partial F)_{ss} = \beta(1 + \chi_1) i_{ss}$ and $(\partial i/\partial P_2)_{ss} = \beta i_{ss}/\varepsilon_0$.

Finally Z_1 may be written

$$Z_1 = \frac{(1/\beta)(1 + \chi_1)^{-1}(s/i_{ss} + \beta_2)}{s + \beta_2 i_{ss}(1 + \chi_1 + \chi_2)(1 + \chi_1)^{-1}} \quad (13)$$

This last expression may be expressed as follows

$$Z_1 = a_0 + a_1 + \frac{a_2}{s + a_3} \quad (14)$$

where

$$\begin{aligned} a_0 &= (1/\beta i_{ss})(1 + \chi_1 + \chi_2)^{-1} \\ a_1 &= (\chi_2/\beta i_{ss})(1 + \chi_1)^{-1}(1 + \chi_1 + \chi_2)^{-1} \\ a_2 &= -(B_2 \chi_2/\beta)(1 + \chi_1)^{-2} \\ a_3 &= -B_2 i_{ss}(1 + \chi_1 + \chi_2)(1 + \chi_1)^{-1} \end{aligned} \quad (15)$$

Since $a_2 < 0$, Z_1 represents an inductive loop with diameter equal to a_1 and displaced along the real axis by a quantity a_0. The characteristic relaxation time constant, τ, is related to a_3 by $1/\tau = -a_3 = 2\pi f_{max}$, where f_{max} represents the frequency at which the imaginary part of Z_1 has a maximum.

Comparing Equations 14 and 15 with 3 the following relations between R_1, R_2 and L with the different parameters involved in Dignam's model are obtained:

$$1 + R_2/R_1 = (1 + \chi_1 + \chi_2)/(1 + \chi_1) \quad (16)$$

$$R_2/L = 1/\tau = B_2 i_{ss}(1 + \chi_1 + \chi_2)/(1 + \chi_1) \quad (17)$$

Figure 5a shows values of $(1 + \chi_1 + \chi_2)/(1 + \chi_1)$ as a function of the applied potential. This relation is not constant but it decreases slightly with decreasing the

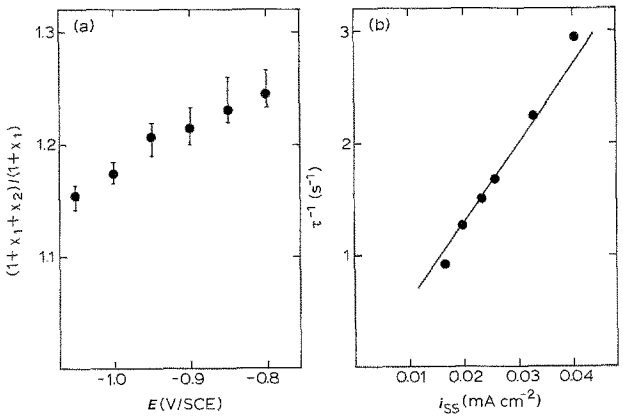

Fig. 5. (a) Potential dependence of the relation between the static and dynamic dielectric constants. Vertical lines indicate the interval of variation of values calculated from independent measurements. (●) Mean values. (b) Current dependence of the characteristic time constant for the inductive loop.

oxide film thickness. Values given in Fig. 5a differ considerably from those calculated by Dignam [3, 7, 8] who reported, for thick oxide films, a relation between the two dielectric constants of ~ 3. One reason for this discrepancy may be the fact that, since our experimental results show a single inductive loop, only the contribution of one slow component (P_2) was taken into account. The other reason may be the different manner of growing the oxide film, which leads to considerable different oxide thicknesses. At this point it is interesting to compare our results with those obtained by other authors. De Wit *et al.* [10] performed impedance measurements on thick aluminium barrier oxide films (δ_{ox} = 100 nm) and they interpreted their results in terms of a surface charge density. However, this model leads to equations of the same form as those developed by Dignam. Taking the data presented by de Wit (Fig. 2 in reference [10]) and applying Equation 16 a ratio between both dielectric constants of ~ 2.6 may be estimated. This value is close to that reported by Dignam for thick oxide films. Bessone *et al.* [13] performed a.c. impedance measurements on aluminium oxide films with a thickness comparable with that obtained under the conditions of the present work. From Fig. 2 in reference [13] and applying Equation 16, increasing values of $(1 + \chi_1 + \chi_2)/(1 + \chi_1)$ from 1.1 to 1.6 may be estimated for $-0.910\,V \leqslant E \leqslant 0.09\,V$. These values are close to those reported in this paper and show a similar dependence with varying the oxide film thickness. This variation may be ascribed to a change of the film structure with formation condition.

Figure 5b represents the potential dependence of the relaxation time τ corresponding to the inductive loop. A linear relation is obtained with a slope of about $7 \times 10^4\,cm^2\,C^{-1}$. Taking a mean value for $(1 + \chi_1 + \chi_2)/(1 + \chi_1)$ of 1.2 and applying Equation 17 a value of $B_2 = 5.8 \times 10^4\,cm^2\,C^{-1}$ is calculated which leads to an interaction radius $r_2 = (B_2\varepsilon_0/\pi)^{1/2}$ of 0.55 nm. This value is consistent with those reported by Dignam for aluminum [3, 7].

The system behaviour at low frequencies showed no evidence of a diffusion-controlled process within the oxide film [11]. This low frequency capacitive loop has not been observed in solutions free from aggressive anions [13] and seems to be directly connected with the presence of Cl^- in the electrolyte. The capacitance, C, related to this loop is about three orders of magnitude greater than C^* (Table 1) and it increases with decreasing potential. This capacitive loop may be ascribed to uniform dissolution of the oxide film before the onset of pitting corrosion, probably, through the formation of chloride containing aluminium complexes which readily go in solution [15–18].

Values of R_3 presented in Table 1 may be discussed in connection with the steady-state curve i_{ss} against E (Fig. 1, inserted subdiagram). According to Equations 2 to 4, it is readily seen that the limit value of Z_F for $\omega \longrightarrow 0$, equals $R_1 + R_3$, which is related to the slope of the steady state curve at each experimental point by $R_1 + R_3 = (di_{ss}/dE)^{-1}$. From Fig. 1 a slope of about $9.5 \times 10^{-5}\,A\,V^{-1}\,cm^{-2}$ was calculated leading to $R_1 + R_3$ values of $10\,500\,\Omega\,cm^{-2}$ in good agreement with those given in Table 1.

Acknowledgements

The authors thank the Consejo Nacional de Investigaciones Científicas y Técnicas (CONICET, Argentina) and the Volkswagen-Stiftung (Germany) for financial support.

References

[1] L. Young, 'Anodic Oxide Films', Academic Press, New York (1961).
[2] V. Brusic, in 'Oxides and Oxide Films' Vol. 1 (edited by J. W. Diggle), Marcel Dekker, New York (1973) ch. 1.
[3] M. J. Dignam, *ibid.*, ch. 2.
[4] H. H. Uhilg, *Corros. Sci.* **19** (1979) 777.
[5] I. Epelboin, C. Gabrielli, M. Keddam and H. Takenouti, in 'Comprehensive Treatise of Electrochemistry' Vol. 4 (edited by J. O'M. Bockris *et al.*), Plenum Press, New York (1981) ch. 3.
[6] N. Sato and G. Okamoto, *ibid.*, ch. 4.
[7] M. J. Dignam, *ibid.*, ch. 5.
[8] D. F. Taylor and M. J. Dignam, *J. Electrochem. Soc.* **120** (1973) 1299, 1306.
[9] R. D. Armstrong and K. Edmondson, *Electrochim. Acta* **18** (1973) 937.
[10] H. J. de Wit, C. Wijenberg and C. Crevecoeur, *J. Electrochem. Soc.* **126** (1979) 779.
[11] C. Y. Chao, L. F. Lin and D. D. Macdonald, *ibid.* **129** (1982) 1874.
[12] S. Ikonopisov, L. Andreeva and C. Vodenicharov, *Electrochim. Acta* **15** (1970) 421.
[13] J. Bessone, C. Mayer, K. Jüttner and W. J. Lorenz, *ibid.* **28** (1983) 171.
[14] M. Keddam, J. F. Lizee, C. Pallota and H. Takenouti, *J. Electrochem. Soc.* **131** (1984) 2016.
[15] Z. A. Foroulis and M. J. Thubrikar, *J. Electrochem. Soc.* **122** (1975) 1296.
[16] T. H. Nguyen and R. T. Foley, *ibid.* **126** (1979) 1855.
[17] R. T. Foley and T. H. Nguyen, *ibid.* **129** (1982) 464.
[18] R. M. Stevanovic, A. R. Despic and D. M. Drazic, *Electrochim. Acta* **33** (1988) 397.